Article

Previous Article | Next Article | Table of Contents

High-Throughput Synthesis and Characterization of $(Ba_xSr_{1-x})_{1+y}Ti_{1-y}O_{3-\delta}$ and $(Ba_xSr_{1-x})_{1+y}Ti_{1-y}O_{3-z}N_z$ Perovskite Thin Films

Anaïs David†, Samuel Guérin*†, Brian E. Hayden†, Robert Noble†, Jean-Philippe Soulié†, Christopher Vian†, Ivoyl P. Koutsaroff‡, Shin'ichi Higai‡, Nobuhiko Tanaka‡, Takehiro Konoike‡, Akira Ando‡, Hiroshi Takagi‡, Teiji Yamamoto‡, Tadao Fukura‡, and Hideharu Ieki‡

† Ilika Technologies, Kenneth Dibben House, Chilworth Science Park, Southampton, SO16 7NS, United Kingdom
‡ Murata Manufacturing Co., Ltd., 10-1 Higashi Kotari 1-chome, Nagaokakyo, Kyoto 617-8555, Japan

Cryst. Growth Des., **2014**, *14* (2), pp 523–532
DOI: 10.1021/cg401259r
Publication Date (Web): December 31, 2013

*E-mail: samuel.guerin@ilika.com.

Special Issue
Published as part of the *Crystal Growth & Design* virtual special issue on Anion-Controlled New Inorganic Materials.

Synopsis

High-throughput synthesis and characterization of $(Ba_xSr_{1-x})_yTi_{1-y}O_{3-z}N_z$ and Gd, Zr codoped $(Ba_xSr_{1-x})_yTi_{1-y}O_{3-z}N_z$ thin film capacitors has led to identification of compositions with the best electrical properties, showing significant improvements in electrical performances compared with $(Ba_xSr_{1-x})_yTi_{1-y}O_3$.

Abstract

Article Options

ACS ActiveView PDF
Hi-Res Print, Annotate, Reference QuickView
PDF (2071 KB)
PDF w/ Links (764 KB)
Full Text HTML

Abstract
Figures
References
Citing Articles

Add to ACS ChemWorx

Add to Favorites
Download Citation

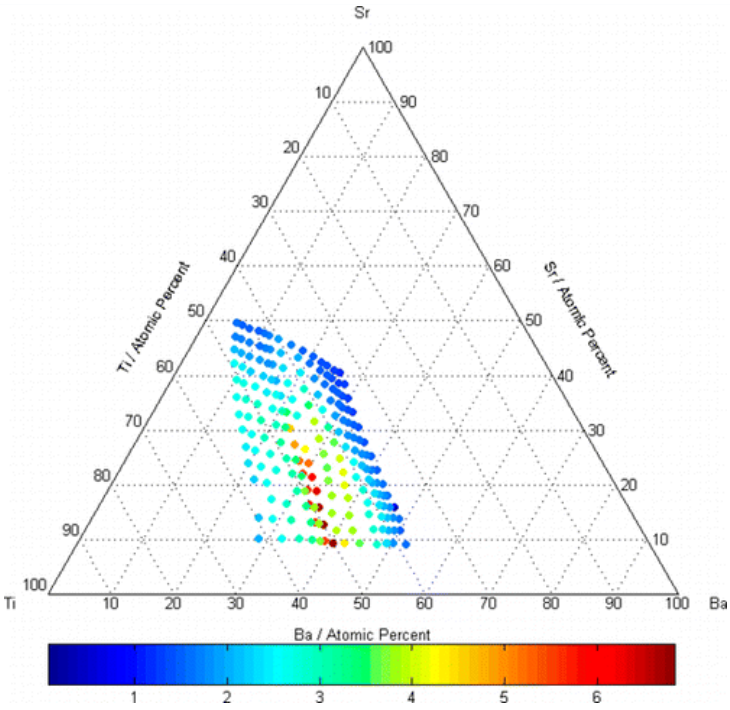

Thin films of $(Ba_xSr_{1-x})_{1+y}Ti_{1-y}$ and Zr, Gd codoped $(Ba_xSr_{1-x})_{1+y}Ti_{1-y}$ were deposited on platinized sapphire substrates at 640 °C under constant flux of atomic oxygen or a mixture of atomic oxygen and nitrogen to synthesize perovskites of $(Ba_xSr_{1-x})_{1+y}Ti_{1-y}O_{3-\delta}$ (also referred to as BSTO), $(Ba_xSr_{1-x})_{1+y}Ti_{1-y}O_{3-z}N_z$ (also referred to as BSTON), and Zr, Gd codoped $(Ba_xSr_{1-x})_{1+y}Ti_{1-y}O_{3-z}N_z$. Structural characterization was done via XRD and XPS, and electrical characterization was done via LCR (dielectric properties and tunability under DC bias) and *P–E* measurements. Although the levels of nitrogen incorporated within the perovskite structure appear to be very low as determined by XPS analysis, definite improvements in dielectric properties and tunability have been achieved by synthesis of the BSTON oxynitride films. For a composition of $Ba_{0.8}Sr_{0.2}TiO_{3-z}N_z$ an improvement by a factor of 1.72 for tunability and 1.44 for relative permittivity has been observed between the oxide and the oxynitride. The oxynitride achieved a tunability ratio of 6.78 to 1 (close to 7:1) under an applied electrical field of 34 kV/mm. The high throughput approach allowed us to highlight a compositional shift for the material with the best dielectric properties when comparing the oxide with the oxynitride thin films. Effects of codoping the perovskite structure with Zr and Gd have also been investigated and although the tunability and dielectric constant of the thin films were not improved, some improvements in dielectric losses were observed, along with a superparaelectric state as observed by *P–E* hysteresis measurements.

View: ACS ActiveView PDF | PDF | PDF w/ Links | Full Text HTML

Citing Articles | Related Content

Citation data is made available by participants in CrossRef's Cited-by Linking service. For a more comprehensive list of citations to this article, users are encouraged to perform a search in SciFinder.

A labile hydride strategy for the synthesis of heavily nitridized BaTiO3
Takeshi Yajima, Fumitaka Takeiri, Kohei Aidzu, Hirofumi Akamatsu, Koji Fujita, Wataru Yoshimune, Masatoshi Ohkura, Shiming Lei, Venkatraman Gopalan, Katsuhisa Tanaka, Craig M. Brown, Mark A. Green, Takafumi Yamamoto, Yoji Kobayashi, Hiroshi Kageyama
*Nature Chemistry***2015** *7* (), 1017-1023

Fabrication and characterization of dielectric strontium titanium oxynitride single crystal
Takuya Hoshina, Akira Sahashi, Hiroaki Takeda, Takaaki Tsurumi
*Japanese Journal of Applied Physics***2015** *54* (), 10NB05

Metal oxynitrides as emerging materials with photocatalytic and electronic properties
Amparo Fuertes
*Mater. Horiz.***2015** *2* (), 453-461

Email a Colleague
Order Reprints
Rights & Permissions
Citation Alerts

SciFinder® Sign in

Retrieve Detailed Record of this Article
Retrieve Substances Indexed for this Article
Retrieve All References Cited for this Article
Retrieve All References Citing this Article

Explore by:
Author of this Article
Any Author
Research Topic

David, Anaïs Search

Metrics

Received 19 August 2013
Published online 31 December 2013
Published in print 5 February 2014

CRYSTAL GROWTH & DESIGN

Article

pubs.acs.org/crystal

High-Throughput Synthesis and Characterization of $(Ba_xSr_{1-x})_{1+y}Ti_{1-y}O_{3-\delta}$ and $(Ba_xSr_{1-x})_{1+y}Ti_{1-y}O_{3-z}N_z$ Perovskite Thin Films

Published as part of the Crystal Growth & Design virtual special issue on Anion-Controlled New Inorganic Materials.

Anaïs David,[†] Samuel Guérin,*[,†] Brian E. Hayden,[†] Robert Noble,[†] Jean-Philippe Soulié,[†] Christopher Vian,[†] Ivoyl P. Koutsaroff,[‡] Shin'ichi Higai,[‡] Nobuhiko Tanaka,[‡] Takehiro Konoike,[‡] Akira Ando,[‡] Hiroshi Takagi,[‡] Teiji Yamamoto,[‡] Tadao Fukura,[‡] and Hideharu Ieki[‡]

[†]Ilika Technologies, Kenneth Dibben House, Chilworth Science Park, Southampton, SO16 7NS, United Kingdom

[‡]Murata Manufacturing Co., Ltd., 10-1 Higashi Kotari 1-chome, Nagaokakyo, Kyoto 617-8555, Japan

ABSTRACT: Thin films of $(Ba_xSr_{1-x})_{1+y}Ti_{1-y}$ and Zr, Gd codoped $(Ba_xSr_{1-x})_{1+y}Ti_{1-y}$ were deposited on platinized sapphire substrates at 640 °C under constant flux of atomic oxygen or a mixture of atomic oxygen and nitrogen to synthesize perovskites of $(Ba_xSr_{1-x})_{1+y}Ti_{1-y}O_{3-\delta}$ (also referred to as BSTO), $(Ba_xSr_{1-x})_{1+y}Ti_{1-y}O_{3-z}N_z$ (also referred to as BSTON), and Zr, Gd codoped $(Ba_xSr_{1-x})_{1+y}Ti_{1-y}O_{3-z}N_z$. Structural characterization was done via XRD and XPS, and electrical characterization was done via LCR (dielectric properties and tunability under DC bias) and *P*−*E* measurements. Although the levels of nitrogen incorporated within the perovskite structure appear to be very low as determined by XPS analysis, definite improvements in dielectric properties and tunability have been achieved by synthesis of the BSTON oxynitride films. For a composition of $Ba_{0.8}Sr_{0.2}TiO_{3-z}N_z$ an improvement by a factor of 1.72 for tunability and 1.44 for relative permittivity has been observed between the oxide and the oxynitride. The oxynitride achieved a tunability ratio of 6.78 to 1 (close to 7:1) under an applied electrical field of 34 kV/mm. The high throughput approach allowed us to highlight a compositional shift for the material with the best dielectric properties when comparing the oxide with the oxynitride thin films. Effects of codoping the perovskite structure with Zr and Gd have also been investigated and although the tunability and dielectric constant of the thin films were not improved, some improvements in dielectric losses were observed, along with a superparaelectric state as observed by *P*−*E* hysteresis measurements.

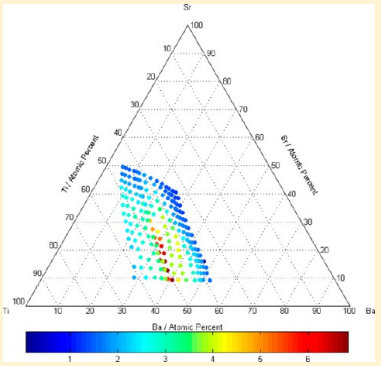

INTRODUCTION

Barium strontium titanate perovskites along the barium to strontium solid solution have been extensively studied due to their interesting electrical properties.[1−16] In the case of thin films, studies have focused on material compositions, synthetic routes, and the influence of the substrate. The main applications of such materials are decoupling capacitors, as well as their potential use in tunable microwave applications. These applications make use of thin film structures; hence research focusing on PVD methods for synthesis are particularly important. Efforts to improve their properties have focused on varying cation ratios and cation substitutions, focusing on compositions along the Ba−Sr tie line, doping either the A-site, the B-site, or both simultaneously, within the perovskite. To date, little effort has been devoted to the study of anion substitutions within the BSTO perovskite, or the effect of simultaneous substitutions of both anions and cations. We have employed a high-throughput approach to their synthesis[17] and characterization, enabling a study of the effects of varying the ratio of the A-site cations along with the ratio of A-site to B-site cations.[18−20] Anion variation was also investigated by the synthesis of barium strontium titanium oxynitride compounds, an extension of early investigations.[21,22]

EXPERIMENTAL SECTION

The thin films were synthesized in a modified MBE system from DCA Instruments. A detailed description of the high throughput deposition method can be found elsewhere.[17] The thin films for electrical characterization were deposited at 640 °C on platinized r-cut sapphire substrates 35 mm × 35 mm fabricated by Murata for the purpose of the study. Thickness measurements were carried out on 35 mm × 35 mm Si ⟨100⟩ substrates from Nova Electronic Materials. Prior to deposition, the substrates were cleaned by sonication in 50%/50% (volume) mixture of ethanol and deionized water for 15 min followed by a further 15 min sonication in pure isopropanol; subsequently the samples were dried under a flux of pure nitrogen and loaded in the vacuum system. The depositions were carried out under ultra high

Received: August 19, 2013
Revised: December 20, 2013
Published: December 31, 2013

vacuum conditions using off-axis sources. Barium pieces from Alfa Aesar 97% (main contaminant Sr) were contained in a Ta crucible and evaporated via a radiative thermal evaporator (Knudsen cell from DCA Instruments). Strontium pieces from Alfa Aesar 99% were contained in a pyrolytic boron nitride crucible and evaporated via a Knudsen cell (DCA Instruments). Titanium slugs 99.98% from Alfa Aesar were contained in a graphite crucible and evaporated via a single pocket 40 cc electron gun (Telemark). For doped thin films, zirconium slugs, 99.9% from Alfa Aesar, were contained in a graphite crucible and evaporated via a single pocket 40 cc electron gun (Telemark), and gadolinium pieces, 99.9% from Testbourne, were loaded in a tungsten crucible and evaporated in a Knudsen cell (DCA Instruments). Wedge shutters for each source were placed in the beam of evaporating material prior to the deposition in order to obtain the compositional spread shown in the present work. Oxygen and nitrogen were supplied to the sample as a uniform mixture of atomic, ionized, and molecular species via an in-line plasma atom source (HD25 from Oxford Applied Research). The ratio of oxygen and nitrogen fed to the atom source was controlled via two mass-flow controllers. The deposition conditions and parameters were optimized to achieve a compositional spread covering the barium rich side of the 50 atom % Ti tie-line and spanning across the tie line. This allows understanding of the influence of A-site to B-site ratio and changes in the ratio of Ba to Sr in the A-site on the properties of the ABO_3 or $ABO_{3-z}N_z$ material all on a single sample. The deposition time was adjusted to achieve a mean thickness of around 170 nm. Due to the nature of the evaporation process and gradient approach, variations in film thicknesses are inevitable. The BSTON thin films showed a variation between 140 and 250 nm. Following deposition, the samples were left to cool under vacuum and taken out. An array of 14 × 14 290 μm diameter platinum top electrodes, with a 2 mm pitch between electrodes, was deposited via DC sputtering in order to create 196 parallel plate capacitors of different BSTO or BSTON compositions. The resulting samples were subsequently annealed in a tube furnace at 650 °C for 30 min under a constant flux of nitrogen. The compositional spread of the thin films was measured using laser ablation inductively coupled mass spectrometry (LA-ICPMS, PerkinElmer ELAN 9000 and New Wave UP213). An array of 8 × 8 measurements equally spaced across the thin film and repeated 3 times was used to obtain the compositional variations of barium, strontium, and titanium and, where applicable, zirconium and gadolinium. The 8 × 8 compositional measurement array was then interpolated to match the array used for electrical and structural studies. For pure oxides and oxynitrides, the concentration of oxygen and oxygen plus nitrogen, respectively, was assumed to be the maximum amount tolerated by the stoichiometry of the perovskite structure. For oxynitride thin films, the relative ratio of oxygen and nitrogen was calculated by X-ray photoelectron spectroscopy (XPS) using a spot XPS (ThermoFisher XR3 twin anode with an Alpha 110 analyzer and the Avantage software). Thin films for XPS were pretreated by Ar^+ etching in order to remove the carbon contaminated top layers. The nitrogen concentration was calculated by comparing the N(1s) and O(1s) XPS signals; the area under each peak was measured using the Avantage software after background subtraction and deconvolution of the signal. Using empirically derived sensitivity factors for XPS,[23] we calculated the relative concentrations by dividing the ratio of the area of the nitrogen peak with its corresponding sensitivity factor by the sum of the ratios of nitrogen area with its sensitivity and of oxygen with its sensitivity. The thickness variations of the thin films was measured by depositing an equivalent sample to those used for structural and electrical characterization through a 14 × 14 contact mask in order to obtain discrete fields for each composition. The film was then coated with a continuous layer of Cu via RF sputtering in order to provide a layer of uniform optical properties. The resulting thin film was analyzed by optical profilometry (Veeco WYKO NT-1100) using an automated procedure providing a map of thickness variations for 196 locations on one sample. Crystallographic information on the different compositions was obtained by X-ray diffraction (XRD) using a 14 × 14 array of diffractograms acquired using a Bruker D8 diffractometer equipped with an Incoatec microsource Cu Kα and GADDS detector. Electrical characterization of the capacitors was carried out using an LCR meter (HP4284A) and a probe station (Signatone) for automated measurements; all electrical measurements were done at 1 kHz using 100 mV AC level with a DC bias varying between ±6 V by 0.5 V steps and starting at 0 V. Polarization−voltage hysteresis curves were also obtained using a Precision RT66B ferroelectric tester from Radiant Technologies. All data collected in high-throughput manner was analyzed and combined using in-house software developed, using MatLab, specifically for our high-throughput studies.

RESULTS AND DISCUSSION

Overall composition and thickness variations for a $(Ba_xSr_{1-x})_{1+y}Ti_{1-y}O_{3-z}N_z$ thin film are presented in Figure 1.

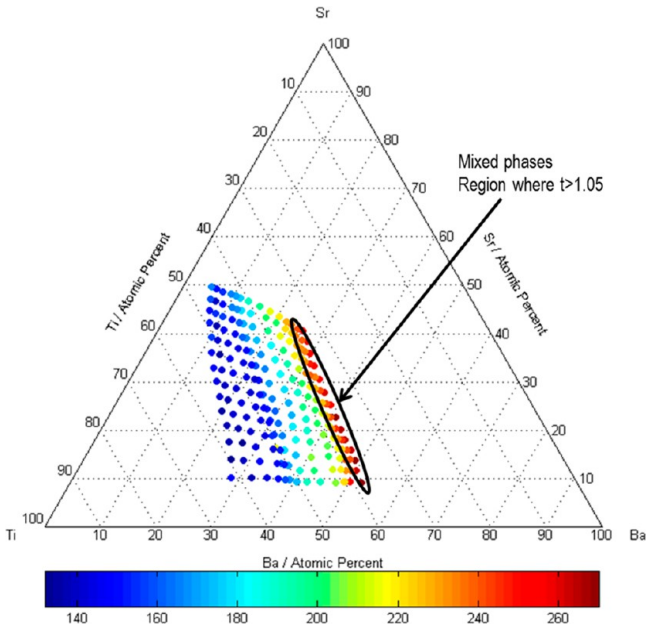

Figure 1. Cationic composition and thickness (color scale in nanometers) variations across a $(Ba_xSr_{1-x})_yTi_{1-y}$ $O_{3-z}N_z$ thin film library deposited on a single platinized sapphire substrate. Single phase perovskite structures were observed by XRD for all compositions apart from those with a large Ti deficiency corresponding to a Goldschmidt's tolerance factor above 1.05.

The compositions cover a large portion of the ternary space and allow understanding of the variations in A-site/B-site ratio as well as Ba to Sr substitution within the perovskite structure. The thin films were deposited at a substrate temperature of 640 °C, allowing for direct crystallization of the material. Attempts were made to deposit the film at lower temperatures, followed by ex situ annealing to ensure crystallization. Although these resulted in crystalline films with the expected perovskite structure, electrical characterization revealed that the capacitors had systematically lower electrical performances than those deposited directly at elevated temperatures. In all cases, XRD reveals the existence of a perovskite structure for a wide range of compositions. Within the range of compositions covered, pure perovskite phase has been observed for compositions with a Goldschmidt's tolerance factor between 0.78 and 1.05, assuming standard ionic radii and using only oxygen as the anion. Where the compositions corresponded to a tolerance factor outside this range, mixed phases were observed; this region is highlighted in Figure 1.

Diffractograms for both $Ba_{0.8}Sr_{0.2}TiO_{3-\delta}$ and $Ba_{0.8}Sr_{0.2}TiO_{3-z}N_z$ thin films are shown in Figure 2 along

dx.doi.org/10.1021/cg401259r | Cryst. Growth Des. 2014, 14, 523−532

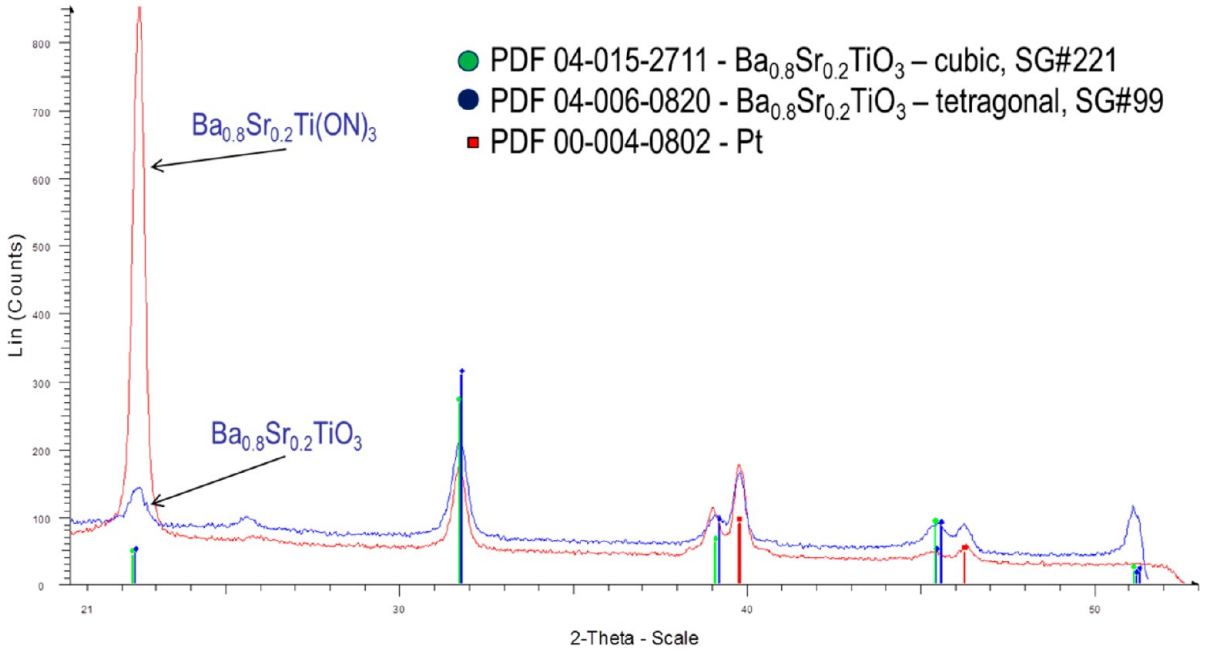

Figure 2. Diffractograms for $Ba_{0.8}Sr_{0.2}TiO_3$ and $Ba_{0.8}Sr_{0.2}TiO_{3-z}N_z$ along with reference data.

with reference patterns for both cubic and tetragonal $Ba_{0.8}Sr_{0.2}TiO_3$ from the ICDD database. There is a clear match between the observed diffractograms and the reference patterns, which can also be indicative of the accuracy of the composition measurements. The relative peak intensities obtained for $Ba_{0.8}Sr_{0.2}TiO_3$ match well those of the reference pattern, whereas those of $Ba_{0.8}Sr_{0.2}TiO_{3-z}N_z$ deviate quite significantly. The oxynitride thin film has a very pronounced (100) preferential orientation. The diffraction frame collected using the GADDS indicates that the oxynitride films possess a highly textured orientation compared with the pure oxide version (see Figure 3d). This observation has been found in all oxynitride thin films. We conclude that the addition of nitrogen during the synthesis leads to a strongly orientated crystal growth. The observed diffractograms (Figure 2) match closely those corresponding to the cubic and tetragonal forms of BSTO; it is not possible to distinguish between the two structures on the basis of the thin film results. A possible distinguishing feature can come from the (111) reflection around 39.1°, which according to the PDF card has the largest shift (0.1103°) of all observed reflections between the two structures. However, the resolution offered by the diffractometer on thin films does not allow a clear answer to be reached apart from the fact that the BSTO and BSTON present different tetragonality.

High-throughput studies enable variations of the structure as a function of composition to be investigated; using the prominent (100) reflection for the BSTON thin film, we map the intensity, the full width at half-maximum (fwhm), and the peak position in Figure 3 (parts a, b, and c, respectively). All these values have been extracted from the XRD data after a Gaussian curve was fitted to each (100) reflection. From Figure 3a, we see that the most intense reflections are recorded for compositions close to $Ba_{0.8}Sr_{0.2}TiO_{3-z}N_z$ but at slightly Ti deficient compositions. The effect of Ti deficiency becomes more pronounced as the barium is substituted for Strontium, although the intensity of the reflection also decreases. The full width at half-maximum is an indicator of the crystallinity of the thin film with the lowest values indicative of a high long-range order. Figure 3b shows that the fwhm ranges from 0.33° to 0.84° with a large central region below 0.4°. This represents the region of best crystallinity, and similarly to what had been observed for the maximum intensity, it covers a region always slightly Ti deficient and defined by all compositions with Ti content between 42 and 50 atom %. The main difference between the two regions is that where the peak maximum deviated to lower Ti concentrations for Sr-rich compositions, no such deviation is observed for the fwhm. On either side of this valley, the fwhm increases because the synthetic conditions and relative concentrations of the elements do not favor the formation of a highly crystalline phase. Finally Figure 3c shows the variation in maximum peak position for the (100) reflection. Focusing on the data along the valley of best crystallinity, the (100) peak position varies from 22.55° to 22.90° as the Ba is substituted with Sr. The shift corresponds to an expected decrease in cell parameters because the ionic radius of Ba is larger than that of Sr in a perovskite A-site coordination. On either side of the region of best crystallinity, but still limited to a region where only the perovskite phase is detected by XRD, the peak position is seen to decrease, indicating an increase in cell parameters probably due to a less ordered crystal structure because defects due to a nonperfect stoichiometry are likely to affect the quality of the long-range order. Further from the region of best crystallinity, for compositions with less than 40% Ti, the peak position increases indicative of a reduction in cell parameters. This reduction is linked to the region where mixed phases are observed by XRD.

In addition to ICPMS and XRD analyses, the thin films were characterized by X-ray photoelectron spectroscopy. The main interest was the quantification of the oxygen to nitrogen ratio to assess the amount of nitrogen incorporated into the perovskite structure but also as a general assessment of the chemical state of the various elements when the oxide and the oxynitride thin films are compared. The peak positions of BSTON thin films for the $Ba(3d_{3/2})$ and $Ba(3d_{5/2})$, $Sr(3d_{3/2})$ and $Sr(3d_{5/2})$, and O(1s) after fitting were determined as, respectively, 795.0 and

dx.doi.org/10.1021/cg401259r | Cryst. Growth Des. 2014, 14, 523−532

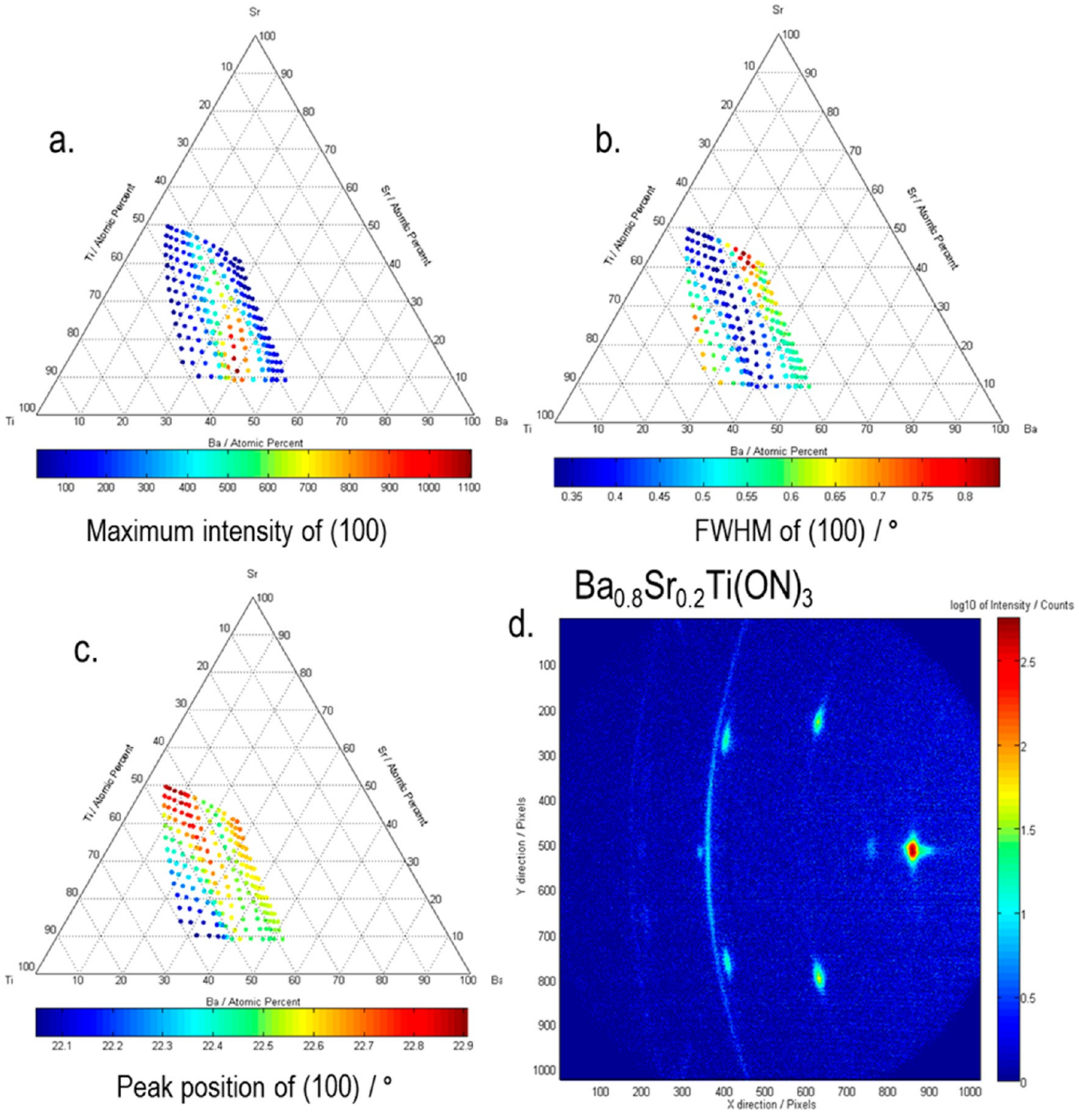

Figure 3. Diffraction characteristics of $(Ba_xSr_{1-x})_yTi_{1-y}O_{3-z}N_z$ thin films. Ternary maps of maximum intensity of (100) reflection (a), full width at half-maximum of (100) reflection (b), and peak position (wrt Cu Kα radiation) of (100) reflection (c). Image of diffraction pattern for $Ba_{0.8}Sr_{0.2}TiO_{3-z}N_z$ (d); the two continuous lines are due to the Pt top electrode (color scale in log of intensity to highlight the various peaks).

779.6 eV, 134.5 and 132.6 eV, and 529.4 eV. This compares to 794.8 and 779.5 eV, 134.4 and 132.5 eV, and 529.2 eV measured for the same peaks on BSTO. We conclude that the incorporation of nitrogen in the film has no significant influence on the chemical environment of these elements. These peaks can be attributed to Ba^{2+}, Sr^{2+}, and O^{2-}, as expected in a perovskite.[21,24−26] These observations have been found to be independent of the compositional variations within the regions where pure perovskites were observed by XRD. For titanium, in the case of BSTON thin films, following the $Ti(2p_{1/2})$ and $Ti(2p_{3/2})$ peaks, some variations were found between two regions delimited by the region of best crystallinity. For composition with a Ti deficiency, a single Ti(2p) doublet is observed at 457.7 and 463.5 eV, whereas for composition with an excess of Ti, a second doublet appears as a shoulder to the main doublet with a binding energy of 455.9 eV for $Ti(2p_{1/2})$ and 461.7 eV for $Ti(2p_{3/2})$. In the case of BSTO thin film only, the doublet at 457.7 and 463.5 eV is observed. It is understood that the main doublet is attributed to Ti^{4+} in the perovskite structure while the second doublet can be attributed to Ti^{3+} in a Ti−N bond.[19,27,28] This observation ties in well with observations made on the N(1s) peak. Figure 4 shows the

dx.doi.org/10.1021/cg401259r | Cryst. Growth Des. 2014, 14, 523−532

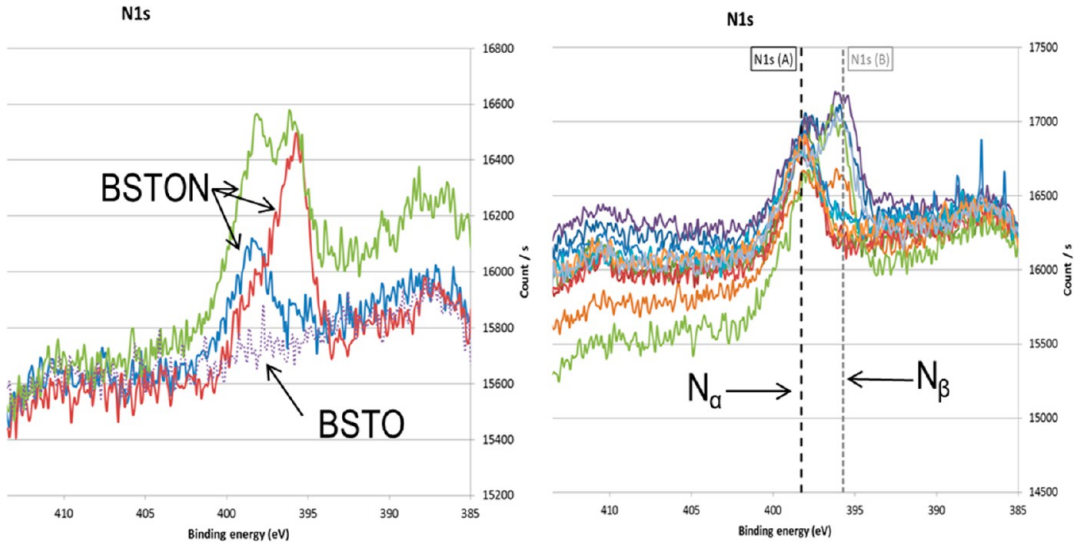

Figure 4. XPS of nitrogen signal from BSTON and BSTO thin films (left) and for various compositions on BSTON thin films (right). N_α is attributed to N substitution in the perovskite oxygen lattice, and N_β is attributed to nitrogen in TiN.

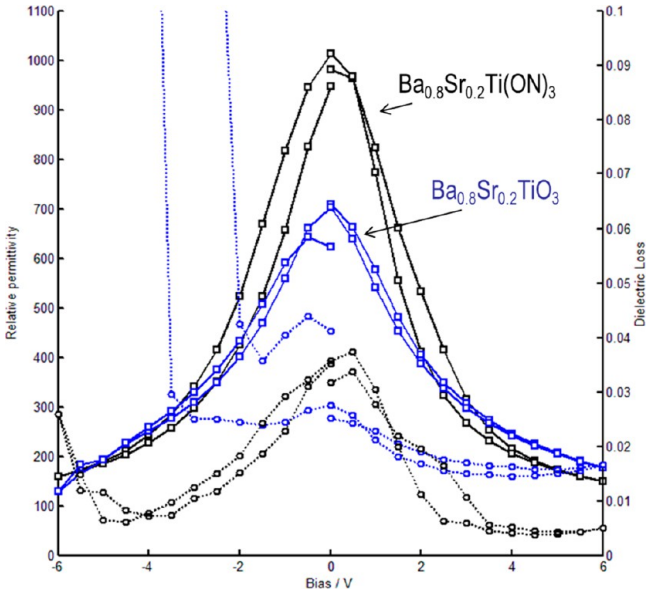

Figure 5. Relative permittivity (solid line) and dielectric loss (dotted line) of $Ba_{0.8}Sr_{0.2}TiO_{3-\delta}$ (blue) and $Ba_{0.8}Sr_{0.2}TiO_{3-z}N_z$ (black) capacitors versus DC bias, as they are measured at 1 kHz, 100 mVac.

N(1s) signal for BSTON thin films for various compositions; the corresponding spectra for the BSTO thin films is also included as a reference. From this, the first observation is that no peak for nitrogen is detected in the case of BSTO. For BSTON, two peaks attributable to nitrogen can be seen, one at 398.3 eV and the second one at 395.7 eV. In the compositional space covered, the peak at 395.7 eV is always observed with the 398.3 eV peak, whereas the 398.3 eV peak is sometime found as a lone peak. Furthermore, the peak at 395.7 eV is observed for titanium rich compositions delimited by the region of highest crystallinity as described for XRD and can therefore be linked to the existence of TiN. Correlating these observations with those of the titanium peaks, the N(1s) the peak at 398.3 eV can be attributed to nitrogen characteristic of a substitution for oxygen within the perovskite structure, and the peak at 395.7 eV to the N^{3-} state typical of a Ti−N bond.[27−31] Furthermore, assuming a linear relationship between binding energy and oxidation state and taking as reference points a binding energy of 402 eV for N^0 (physisorbed) and 396 eV for N^{3-}, we can estimate the oxidation state of the N(1s) signal at 398.3 eV to correspond to N^{2-}.

Using the N(1s) peak attributed to the oxynitride bond and the O(1s) peak, we found the estimated nitrogen content in the thin film to be very low. The average nitrogen content was found to vary between 0.007 and 0.023 atom % for samples made using different oxygen to nitrogen ratio. The highest average was obtained for a film made with oxygen to nitrogen ratio at synthesis of 1:3. Within the same BSTON sample, the measured concentration of nitrogen was also found to vary as a function of composition. In the case of the BSTON sample with the average nitrogen content of 0.023 atom %, the variation was found to be between 0.012 and 0.047 atom %. Further work would be required to fully understand the different interactions taking place between the relative amount of gas (oxygen and nitrogen partial pressures) being fed during synthesis at high temperatures, the total amount of gas against the deposition rate, and the nitrogen reactivity with the different elements (Ba, Sr, Ti). Since each element has a different affinity for the gases, variations in composition of these elements across the thin film can lead to the variations of oxygen to nitrogen ratio observed.

Despite the low nitrogen levels, the oxynitride BSTON thin films possess better electrical characteristics than the oxides. Furthermore, the thin films prepared with the lowest oxygen to nitrogen ratio (1 to 3) did not perform as well as those made with a 1 to 2 ratio. Comparison of the electrical performances of the BSTON oxynitride and the BSTO oxide thin film is usually presented for very similar compositions of barium ($0.6 < Ba < 0.8$), strontium ($0.4 < Sr < 0.2$), and titanium ($0.9 < Ti < 1.05$).[22] Our high throughput data enables us to compare capacitors of similar composition, as well as comparing the best oxynitride capacitor against the best oxide capacitor within the compositional spread covered. This is essential since our data reveals that the best electrical properties from the oxynitride BSTON films do not correspond to the same composition as the best electrical properties of the oxide BSTO films. Focusing first on identical composition, Figure 5 shows the relative

dx.doi.org/10.1021/cg401259r | Cryst. Growth Des. 2014, 14, 523−532

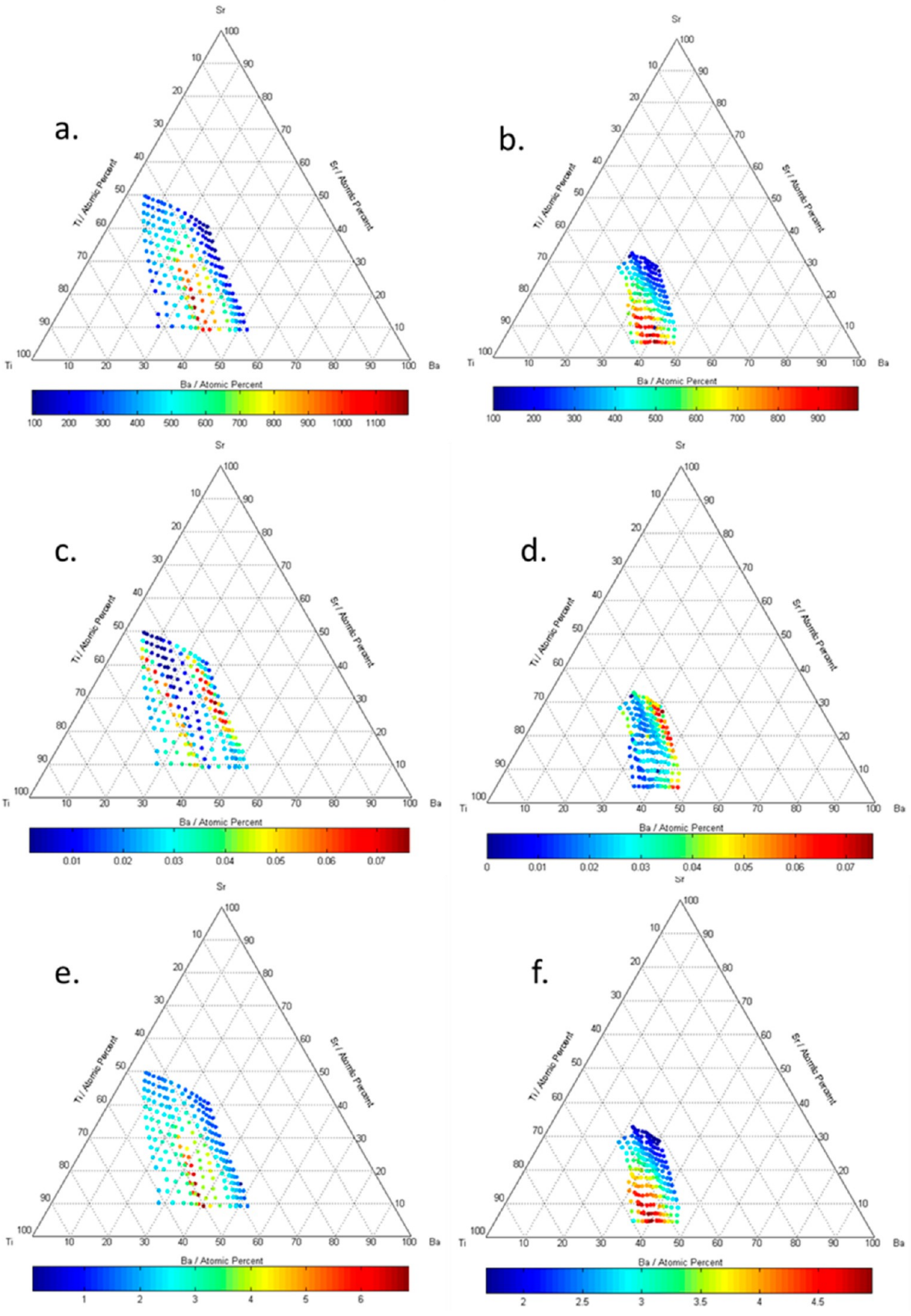

Figure 6. Ternary plots of the dielectric characteristics of BSTO and BSTON thin films measured at 1 kHz, 100 mVac. Relative permittivity for BSTON (a) and BSTO (b), dielectric loss for BSTON (c) and BSTO (d), tunability at 6 V/0 V for BSTON (e) and BSTO (f).

dx.doi.org/10.1021/cg401259r | *Cryst. Growth Des.* 2014, 14, 523−532

Table 1. Comparison of Capacitor Structures with Highest Relative Permittivity and Highest Tunability from $(Ba_xSr_{1-x})_{1+y}Ti_{1-y}O_3$ and $(Ba_xSr_{1-x})_{1+y}Ti_{1-y}O_{3-z}N_z$

	BSTO		BSTON	
	highest ε_r	highest tunability	highest ε_r	highest tunability
Ti atom %	53.6	55.9	49.5	49.9
Ba atom %	41.5	37.1	34.5	37.5
Sr atom %	4.9	7.0	16.0	12.6
ε_r (1 kHz) at 0 V	996	883	1191	1111
tunability at 6 V	4.7	4.9	6.5	6.8
tan δ (1 1 kHz) at 0 V	0.0217	0.0161	0.0245	0.032
tan δ (1 kHz) at 6 V	0.0129	0.018	0.0032	0.0034

permittivity and dielectric loss against applied DC field for both $Ba_{0.8}Sr_{0.2}TiO_{3-\delta}$ and $Ba_{0.8}Sr_{0.2}TiO_{3-z}N_z$. A clear improvement in electrical properties can be seen for the oxynitride with a relative permittivity of 1012 against 702 for the oxide, both at 0 V at 1 kHz, representing an improvement factor of 1.44. The dielectric loss is slightly higher at 0 V for the oxynitride (tan δ = 0.037) than the oxide (tan δ = 0.028) but becomes very low at higher DC bias with tan δ reaching 0.005 for an electrical field of 34 kV mm^{-1}, whereas it remains at 0.017 at 36 kV mm^{-1} for the oxide. Interestingly, the oxynitride has lower leakage currents under both DC polarities (±6 V); this is not the case for the oxide, which displays a large leakage current on the reverse polarity. The tunability ratio of each capacitor was calculated by dividing the relative permittivities at 0 V and at 6 V. A value of 6.78:1 (6 V) was obtained for the oxynitride against a value of 3.94:1 (6 V) for the oxide grown at the same substrate temperature to a similar film thickness. This corresponds to an improvement of 1.72 and is much higher than any reported voltage tunability for BSTO films under dc biases of 6 V.[15,16,32] This improvement could be attributed to the small addition of nitrogen into the perovskite structure or to an improvement of the crystallographic arrangement caused by the synthesis in the presence of atomic nitrogen as observed in XRD. The Gd, Zr codoped BSTON system shown later in the present manuscript possesses a crystallographic structure similar to that of the BSTON (i.e., strongly textured (100) preferential orientation) and lower dielectric properties, we can therefore suggest that the improvements seen for the BSTON are due to the addition of nitrogen and not to the crystal arrangement. There is, therefore, a significant improvement in

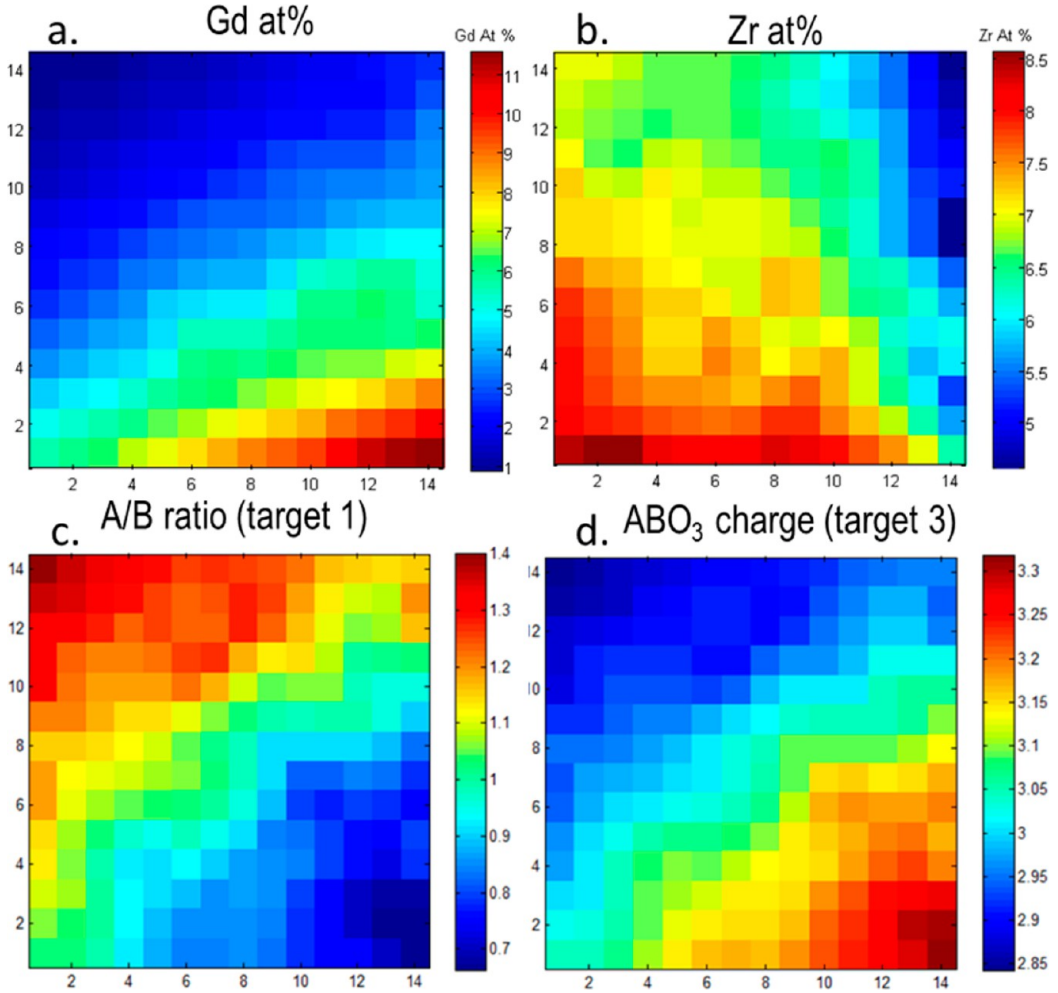

Figure 7. Array (14 ×14) maps of the compositional cationic characteristics of $(Ba_{0.8-x}Gd_xSr_{0.2})_{1+y}(Ti_{1-p}Zr_p)_{1+y}O_{3-z}N_z$ created on a single substrate. Variations of Gd atomic concentration (a), Zr atomic concentration (b), A-site to B-site ratio (c) (balanced target of 1), and charge of cationic sublattice or ABO_3 charge balance (d) (target of 3 for a balanced ABO_3 perovskite) . The x and y coordinates denote different positions on the array/substrate.

dx.doi.org/10.1021/cg401259r | Cryst. Growth Des. 2014, 14, 523−532

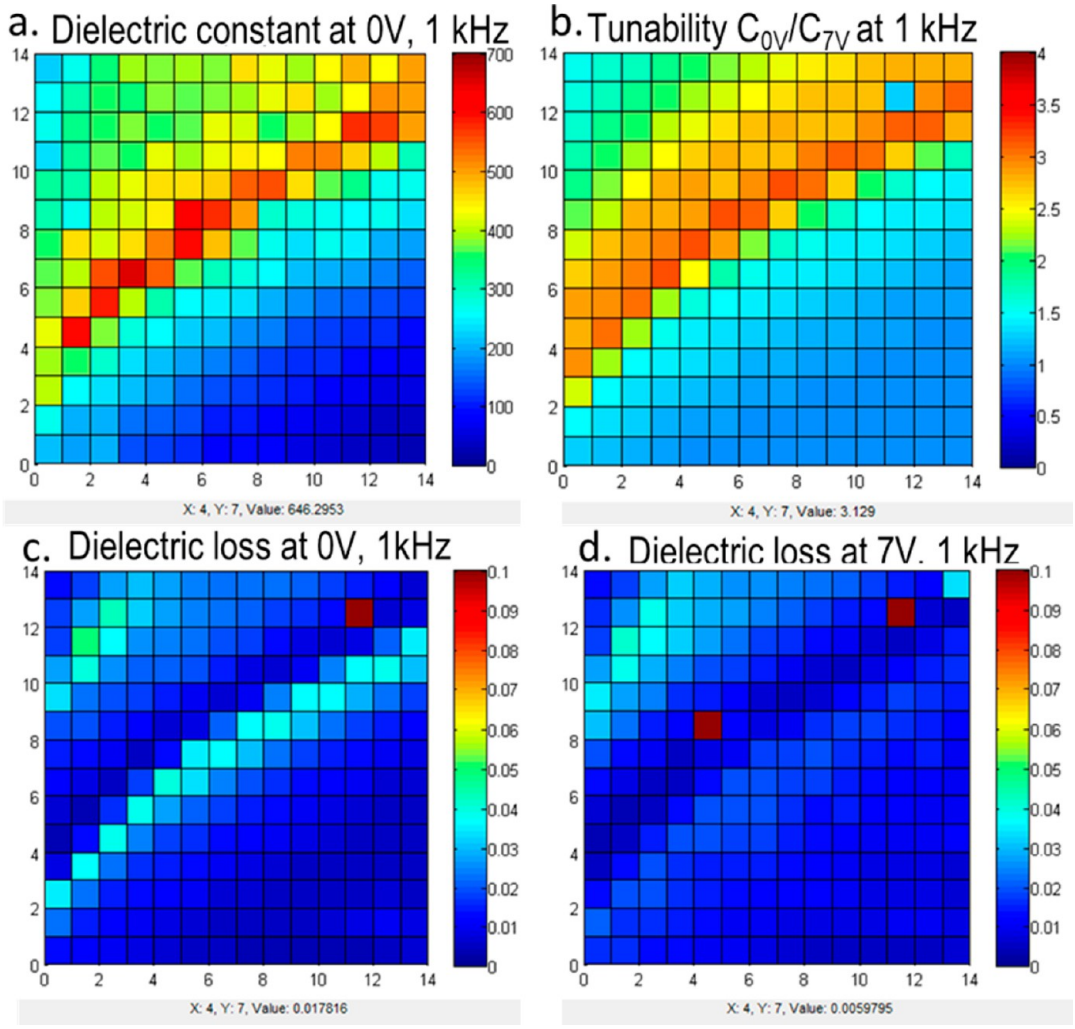

Figure 8. Maps of the characteristics of 14 × 14 array capacitors of $(Ba_{0.8-x}Gd_xSr_{0.2})_{1+y}(Ti_{1-p}Zr_p)_{1+y}O_{3-z}N_z$ created on a single substrate. Variations of relative permittivity (a), tunability as the ratio of relative permittivity at 0 and 7 V (b), dielectric loss at 0 V (c), and dielectric loss at 7 V (d). The x and y coordinates denote different positions on the array/substrate.

electrical properties between a pure oxide perovskite of barium, strontium and titanium and its corresponding oxynitride. Analysis of the data collected across the compositional spread covered reveals some significant differences between the two systems (BSTO vs BSTON) in terms of compositional regions of high electrical performance. Figure 6 summarizes the electrical characteristics as a function of composition: Figure 6a,b shows the variations in relative permittivity at 1 kHz and 0 V DC bias for the oxynitride and the oxide as a function of composition, respectively. The clear difference is that the region of highest relative permittivity for the oxide corresponds to compositions with Ti ≥ 50 atom %, whereas it is for compositions with Ti ≤ 50 atom % in the oxynitride system. In both cases, the ratio Ba/Sr = 4 seems to correspond to the most optimal region; however some deviations from this exact figure are tolerated. Importantly the trends in Figure 6a bear a strong resemblance to the trends of the maximum intensity of the (100) reflection from XRD (Figure 3a). Across all samples and for all systems measured there is always a clear link between the most intense reflections from XRD and the best electrical properties. However, a maximum in XRD intensity is a necessary but not a sufficient indicator of a material suitable for the best capacitor, in terms of relative permittivity or tunability. Second, Figure 6c,d shows the variations in dielectric loss at 1 kHz under 0 V DC bias for, respectively, the oxynitride and the oxide as a function of composition. The same regions of interest, in terms of Ti concentration, as those found for the relative permittivity are observable. The dielectric loss falls to lower values for the oxynitride than for the oxide, with the Sr rich part of the compositional spread possessing the lowest values. For the oxide, no such trend is apparent within the compositional spread covered. Finally, Figure 6e,f shows the variations in tunability between 0 and 6 V at 1 kHz for, respectively, the oxynitride and the oxide as a function of composition. Again the same observation in terms of Ti concentration can be made, with the oxynitride achieving the highest tunability for Ti ≤ 50 atom % and the oxide for Ti ≥ 50 atom %. The range of relatively high tunability covers a fairly broad range of compositions for the oxide, whereas it is limited to a narrow compositional range for the oxynitride. In fact, only 12 capacitors out of 196 have tunability above 5 for the oxynitride, whereas in the case of the oxide 33 out of 196 have tunability above 4. Table 1 summarizes the best electrical data recorded along with the corresponding composition. It highlights the differences between the oxynitride and the

dx.doi.org/10.1021/cg401259r | Cryst. Growth Des. 2014, 14, 523−532

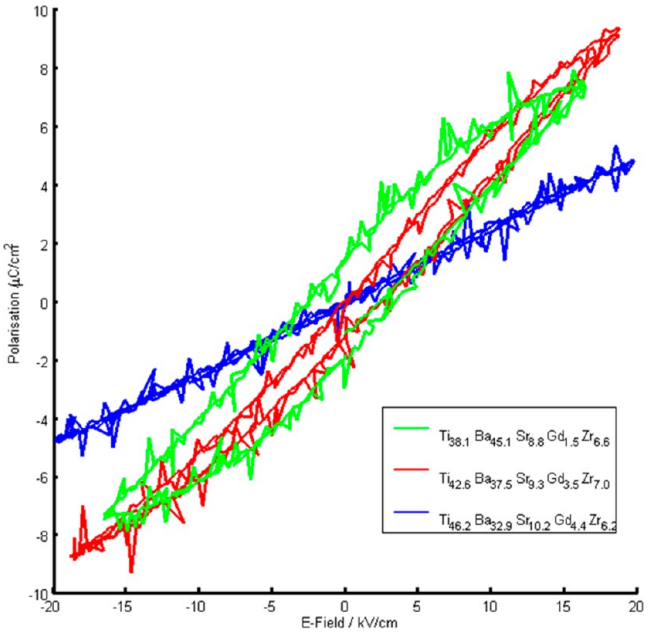

Figure 9. *P*−*E* hysteresis loops for GdZr codoped $(Ba_xSr_{1-x})_{1+y}Ti_{1-y}O_{3-z}N_z$ thin film capacitors. In blue for a B site rich perovskite, in red for nearly balanced perovskite and in green for A-site rich perovskite.

oxide as well as the fact that the highest relative permittivity does not correspond to the highest tunability.

Focusing on the $Ba_{0.8}Sr_{0.2}TiO_{3-z}N_z$ composition, we synthesized some thin films codoped with gadolinium and zirconium. The arrangement of the sources and their evaporation characteristics were optimized to allow the Zr to gradually replace the Ti as a B site dopant and the Gd to take the place of the Ba (the majority A-site element). For the sample described in the present study, the gadolinium concentration was varied from 0.9 to 11.6 atom % and the zirconium concentration varied from 4.6 to 8.6 atom % across the array (see Figure 7a,b). Calculations using the relative concentrations of the elements along with assumed charges and site occupancies in the perovskite structure enable us to assess for which part of the sample the conditions are optimal for the formation of the perovskite. These calculations are represented in Figure 7c,d and show, respectively, the ratio A-site to B-site and the charge balance of the ABO_3 perovskite structure. In case of the charge balance, the oxidation states were assumed to be Ti^{4+}, Zr^{4+}, Ba^{2+}, Sr^{2+}, and Gd^{3+} (the most common oxidation state of Gd), thus creating a slight disparity between the band of A/B ratio equal to 1 and the band of charge of the cationic sublattice (also referred as ABO_3 charge) equal to 3. From both maps, the regions matching the target values fall as a line stretching diagonally across the sample. XRD of the sample revealed a perovskite structure spanning the entire compositional spread with a strong (100) preferential orientation similar to what has been observed for undoped oxynitride samples. Electrical characterization of the thin film was carried out, and the results are summarized in Figure 8a−d. The relative permittivity and the tunability of the Zr, Gd codoped thin films is lower than even BSTO with values of, respectively, 646 and 3.1 at 7 V (corresponding to comparable electrical field for BSTO and BSTON samples). Hence as a general comment, no significant improvement in electrical performance is found when the BSTON is doped with both Gd and Zr. However, Figure 8c,d shows the variation of dielectric loss across the sample at, respectively, 0 and 7 V. The overall level of dielectric loss is lower than what had been observed for BSTO or BSTON and the whole compositional spread covered retains a very low dielectric loss at 1 kHz under 7 V DC bias. Therefore, the main benefit of the codoping, for this BSTON system and under our synthetic route, is a significant lowering of the dielectric loss as well as a general gain in stability under high electrical field. A more detailed reading of the map for the relative permittivity (Figure 8a) also shows that the band of highest values falls along the line of a balanced charge of the cationic sublattice (ABO_3 on target) and not on the line of A/B ratio on target. This is an important observation because it indicates that the charge balance is more important than the A-site to B-site ratio. The same observation is true for the tunability map shown in Figure 8b. Finally, the relative permittivity is seen to decrease sharply to low values for B-site rich compositions (corresponding also to excess cation charges) and fades more gently for A-site rich compositions (deficiency in cation charge).

Investigation of the polarization of the thin films against electric field was done using a ferroelectric tester for the GdZr doped BSTON films. Characteristics that can be linked to the A-site to B-site ratio and charge balance have been observed and are shown in Figure 9. For the limited electrical field applied, the capacitors with excess B site elements (therefore with excess cation charge) display a response typical of a pure dielectric material with a linear change in polarization as the electrical field changes. Capacitors with excess A-site elements (deficient in overall cation charge) show a response more akin to a ferroelectric material. Capacitors with a ratio of A-sites to B-sites close to one have a response closer to a superparaelectric state, with a saturation in polarization at higher electrical fields and relatively little remnant polarization at 0 V. Interestingly the example shown in Figure 9 has an A/B ratio close to one (1.01) but a charge balance slightly above the target of 3 (3.025); another capacitor (not shown) with an A/B ratio of 1.10 but a charge balance closer to the target of 3 (2.987) has an even more pronounced superparaelectric state with a smaller remnant polarization than the capacitor shown in Figure 9. This highlights the importance of the charge balance when dealing with doping the oxynitride perovskite structure with cations of different oxidation state than those they are replacing.

CONCLUSIONS

Oxide and oxynitride thin films of $(Ba_xSr_{1-x})_yTi_{1-y}O_{3-z}N_z$ and ZrGd codoped $(Ba_xSr_{1-x})_{1+y}Ti_{1-y}O_{3-z}N_z$ were deposited on platinum-coated Al_2O_3 substrates and characterized by XRD and electrical measurements. The addition of nitrogen into BSTO leads to a highly textured (100) preferential orientation crystal structure. Electrical characterization revealed that the oxynitride BSTON outperforms the oxide BSTO by a factor of 1.44 for dielectric constant at 0 V and by 1.68 for the voltage tunability at ∼35 kV mm^{-1} for samples deposited at the same substrate temperature and to similar thicknesses. In addition to the anion substitution by adding the nitrogen, we also doped the cations on both sites of the perovskite by adding Gd and Zr simultaneously. The electrical performances of the codoped BSTON thin films showed that the improvements are about a lowering of the dielectric loss and significantly extended tan δ stability under 6−7 V dc biases. The overall voltage tunability and relative permittivity of the codoped BSTON were found to

dx.doi.org/10.1021/cg401259r | *Cryst. Growth Des.* 2014, 14, 523−532

be lower than in the case of the BSTON. Indications of the variations between ferroelectric region, superparaelectric, and linear paraelectric (dielectric) region were shown in relation to the charge balance and A-site to B-site ratio of the perovskite structure. This paper also demonstrates that the high-throughput synthesis and screening approach is well suited for the study of anionic and cationic substitutions within a well-defined crystal structure.

AUTHOR INFORMATION

Corresponding Author

*E-mail: samuel.guerin@ilika.com.

Notes

The authors declare no competing financial interest.

REFERENCES

(1) Bouyanfif, H.; Wolfman, J.; El Marssi, M.; Yuzyuk, Y.; Bodeux, R.; Gervais, M.; Gervais, F. Combinatorial (Ba,Sr)TiO_3 thin film growth: X-ray diffraction and Raman spectroscopy. *J. Appl. Phys.* **2009**, *106* (3), No. 034108.

(2) Hong, S.; Bak, H.; An, I.; Kim, O. K. Microstructural and electrical properties of $Ba_xSr_{1-x}TiO_3$ thin films on various electrodes. *Jpn. J. Appl. Phys., Part 1* **2000**, *39* (4A), 1796−1800.

(3) Ito, S.; Funakubo, H.; Koutsaroff, I. P.; Zelner, M.; Cervin-Lawry, A. Effect of the thermal expansion matching on the dielectric tunability of (100)-one-axis-oriented $(Ba_{0.5}Sr_{0.5})TiO_3$ thin films. *Appl. Phys. Lett.* **2007**, *90* (14), No. 142910.

(4) Ito, S.; Takahashi, K.; Okamoto, S.; Koutsaroff, I. P.; Cervin-Lawry, A.; Funakubo, H. Orientation dependence of epitaxial and one-axis-oriented $(Ba_{0.5}Sr_{0.5})TiO_3$ films prepared by RF magnetron sputtering. *Jpn. J. Appl. Phys., Part 1* **2005**, *44* (9B), 6881−6884.

(5) Ito, S.; Yamada, T.; Takahashi, K.; Okamoto, S.; Kamo, T.; Funakubo, H.; Koutsaroff, I.; Zelner, M.; Cervin-Lawry, A. Effect of bottom electrode on dielectric property of sputtered-(Ba,Sr)TiO_3 films. *J. Appl. Phys.* **2009**, *105* (6), No. 061606.

(6) Koutsaroff, I. P.; Bernacki, T. A.; Zelner, M.; Cervin-Lawry, A.; Jimbo, T.; Suu, K. Characterization of thin-film decoupling and high-frequency (Ba,Sr)TiO_3 capacitors on Al_2O_3 ceramic substrates. *Jpn. J. Appl. Phys., Part 1* **2004**, *43* (9B), 6740−6745.

(7) Mahani, R. M.; Battisha, I. K.; Aly, M.; Abou-Hamad, A. B. Structure and dielectric behavior of nano-structure ferroelectric $Ba_xSr_{1-x}TiO_3$ prepared by sol-gel method. *J. Alloys Compd.* **2010**, *508* (2), 354−358.

(8) Qin, W. F.; Xiong, J.; Zhu, J.; Tang, J. L.; Jie, W. J.; Wei, X. H.; Zhang, Y.; Li, Y. R. High tunabilty $Ba_{0.6}Sr_{0.4}TiO_3$ thin films fabricated on Pt-Si substrates with $La_{0.5}Sr_{0.5}CoO_3$ buffer layer. *J. Mater. Sci.: Mater. Electron.* **2008**, *19* (5), 429−433.

(9) Simoes, A. Z.; Moura, F.; Onofre, T. B.; Ramirez, M. A.; Varela, J. A.; Longo, E. Microwave-hydrothermal synthesis of barium strontium titanate nanoparticles. *J. Alloys Compd.* **2010**, *508* (2), 620−624.

(10) Wang, D. Y.; Wang, Y.; Dai, J. Y.; Chan, H. L. W.; Choy, C. L. Substrate effect on in-plane ferroelectric and dielectric properties of $Ba_{0.7}Sr_{0.3}TiO_3$ thin films. *J. Electroceram.* **2006**, *16* (4), 587−591.

(11) Zhu, X.; Chan, H. L. W.; Choy, C. L.; Wong, K. H.; Xu, J.; Shi, S. Preparation of epitaxial compositionally graded $(Ba_{1-x}Sr_x)TiO_3$ thin films with enhanced dielectric properties. *Appl. Phys. A: Mater. Sci. Process.* **2003**, *77* (3−4), 499−505.

(12) Zhu, X. H.; Guigues, B.; Defay, E.; Dubarry, C.; Aid, M. Low temperature perovskite crystallization of highly tunable dielectric $Ba_{0.7}Sr_{0.3}TiO_3$ thick films deposited by ion beam sputtering on platinized silicon substrates. *J. Appl. Phys.* **2009**, *105* (4), No. 044108.

(13) Padmini, P.; Taylor, T. R.; Lefevre, M. J.; Nagra, A. S.; York, R. A.; Speck, J. S. Realization of high tunability barium strontium titanate thin films by rf magnetron sputtering. *Appl. Phys. Lett.* **1999**, *75* (20), 3186−3188.

(14) Pervez, N. K.; Hansen, P. J.; York, R. A. High tunability barium strontium titanate thin films for rf circuit applications. *Appl. Phys. Lett.* **2004**, *85* (19), 4451−4453.

(15) Cross, J. S.; Koutsaroff, I. P. Review on ferroelectric thin film devices: Fundamental aspects and integration challenges. *Taikabutsu* **2010**, *62* (4), 162−174.

(16) Lu, S. B.; Xu, Z. K. Internal residual stress studies and enhanced dielectric properties in $La_{0.7}Sr_{0.3}CoO_3$ buffered (Ba, Sr)TiO_3 thin films. *J. Appl. Phys.* **2009**, *106* (6), No. 064107.

(17) Guerin, S.; Hayden, B. E. Physical vapor deposition method for the high-throughput synthesis of solid-state material libraries. *J. Comb. Chem.* **2006**, *8* (1), 66−73.

(18) Devi, S.; Jha, A. K. Structural, dielectric and ferroelectric studies of tungsten substituted barium strontium titanate. *Ferroelectrics* **2010**, *402*, 168−174.

(19) Fan, Y. H.; Yu, S. H.; Sun, R.; Li, L.; Yin, Y. S.; Wong, K. W.; Du, R. X. Microstructure and electrical properties of Mn-doped barium strontium titanate thin films prepared on copper foils. *Appl. Surf. Sci.* **2010**, *256* (22), 6531−6535.

(20) Liu, G. Z.; Wolfman, J.; Autret-Lambert, C.; Sakai, J.; Roger, S.; Gervais, M.; Gervais, F. Microstructural and dielectric properties of $Ba_{0.6}Sr_{0.4}Ti_{1-x}Zr_xO_3$ based combinatorial thin film capacitors library. *J. Appl. Phys.* **2010**, *108* (11), No. 114108.

(21) Gao, Y. H.; Shen, H.; Ma, J. H.; Xue, J. Q.; Sun, J. L.; Meng, X. J.; Chu, J. H.; Wang, P. N. Surface chemical composition and optical properties of nitrogen-doped $Ba_{0.6}Sr_{0.4}TiO_3$ thin films. *J. Appl. Phys.* **2007**, *102* (6), No. 064106.

(22) Koutsaroff, I. Presented at the Symposium 6 (Advances in Electro Ceramics), ICC3, Osaka, Japan, Nov 14−18 2010, 2010; Osaka, Japan, 2010, S6-006.

(23) Wagner, C. D.; Davis, L. E.; Zeller, M. V.; Taylor, J. A.; Raymond, R. H.; Gale, L. H. Empirical atomic sensitivity factors for quantitative-analysis by electron-spectroscopy for chemical-analysis. *Surf. Interface Anal.* **1981**, 3 (5), 211−225.

(24) Craciun, V.; Singh, R. K. Characteristics of the surface layer of barium strontium titanate thin films deposited by laser ablation. *Appl. Phys. Lett.* **2000**, *76* (14), 1932−1934.

(25) Lu, H.; Pan, J. S.; Chen, X. F.; Zhu, W. G.; Tan, O. K. Influence of annealing temperature on the band structure of sol-gel $Ba_{0.65}Sr_{0.35}TiO_3$ thin films on n-type Si(100). *Appl. Phys. Lett.* **2006**, *88* (13), No. 132907.

(26) Nasser, S. A. X-ray photoelectron spectroscopy study on the composition and structure of $BaTiO_3$ thin films deposited on silicon. *Appl. Surf. Sci.* **2000**, *157* (1−2), 14−22.

(27) Feng, L. W.; Chang, C. Y.; Chang, T. C.; Tu, C. H.; Wang, P. S.; Lin, C. C.; Chen, M. C.; Huang, H. C.; Gan, D. S.; Ho, N. J.; Chen, S. C. Formation and composition of titanium oxinitride nanocrystals synthesized via nitridizing titanium oxide for nonvolatile memory applications. *Thin Solid Films* **2011**, *519* (22), 7977−7981.

(28) Saha, N. C.; Tompkins, H. G. Titanium nitride oxidation chemistry - An X-ray photoelectron spectroscopy study. *J. Appl. Phys.* **1992**, *72* (7), 3072−3079.

(29) Mi, Y. Y.; Wang, S. J.; Chai, J. W.; Pan, J. S.; Huan, C. H. A.; Feng, Y. P.; Ong, C. K. Effect of nitrogen doping on optical properties and electronic structures of $SrTiO_3$ films. *Appl. Phys. Lett.* **2006**, *89* (23), No. 231922.

(30) Mi, Y. Y.; Yu, Z.; Wang, S. J.; Gao, X. Y.; Wee, A. T. S.; Ong, C. K.; Huan, C. H. A. Thermal stability of nitrogen-doped $SrTiO_3$ films: Electronic and optical properties studies. *J. Appl. Phys.* **2007**, *101* (6), No. 063708.

(31) Simon, P.; Pignon, B.; Miao, B.; Coste-Leconte, S.; Leconte, Y.; Marguet, S.; Jegou, P.; Bouchet-Fabre, B.; Reynaud, C.; Herlin-Boime, N. N-doped titanium monoxide nanoparticles with TiO rock-salt structure, low energy band gap, and visible light activity. *Chem. Mater.* **2010**, *22* (12), 3704−3711.

(32) Spartak, G. *Ferroelectrics in Microwave Devices, Circuits and Systems Physics, Modeling, Fabrication and Measurements*; Springer: London, 2009.